



Simulation of transient convective burning of an n-octane droplet using a four-step reduced mechanism

Guang Wu^{a,*}, William A. Sirignano^a, Forman A. Williams^b

^a Department of Mechanical and Aerospace Engineering, University of California, Irvine, CA 92697-3975, United States

^b Department of Mechanical and Aerospace Engineering, University of California, San Diego, CA 92093-0411, United States

ARTICLE INFO

Article history:

Received 17 August 2010

Received in revised form 7 November 2010

Accepted 7 November 2010

Available online 7 December 2010

Keywords:

Transient burning

Convection

Four-step reduced mechanism

Flame transition

ABSTRACT

The transient burning of an n-octane fuel droplet in a hot gas stream is numerically studied using a four-step reduced mechanism, with considerations of droplet surface regression, deceleration due to the drag of the droplet, internal circulation inside the droplet, variable properties, non-uniform surface temperature, and the effect of surface tension. Two different types of the four-step mechanism are examined and found almost identical. The four-step mechanism has earlier instant of the wake-to-envelope transition than the one-step mechanism at low ambient temperature, but this difference between the two mechanisms diminishes when the ambient temperature is increased. The four-step mechanism has smaller mass burning rate for a wake flame but greater mass burning rate for an envelope flame than the one-step mechanism. The two mechanisms have small differences in the critical initial Damkohler number. Lower ambient temperature yields later wake-to-envelope transition and smaller mass burning rate. Higher ambient pressure has greater overall mass burning rate because of greater gas density and thus greater concentrations of reactants for a major part of the lifetime. Greater ambient mass fraction of oxygen yields faster oxidation kinetics and greater Damkohler number. As the ambient mass fraction of oxygen increases, the instant of wake-to-envelope transition advances for an initial wake flame, and finally the initial flame becomes an envelope flame when the ambient mass fraction of oxygen exceeds some critical value. A correlation is developed for the critical initial Damkohler number in terms of the ambient temperature, ambient pressure, and ambient mass fraction of oxygen.

Published by Elsevier Inc. on behalf of The Combustion Institute.

1. Introduction

The studies of droplet vaporization and burning in a spray can be applied in the design of rocket, ramjet, gas turbine combustors and furnaces to predict combustor performance, stability, and pollutant emissions for these combustors. One feature of a real spray is gas–stream convection. The gas–stream convection complicates the studies by requiring solutions of the flow field, the internal circulation, and the non-uniform surface temperature.

Prakash and Sirignano [1,2] used a vortex model to approximate the internal motion in the liquid phase. An integral approach was applied to approximate the solutions for the boundary layer around the droplet interface. The analysis indicated that the droplet heating and vaporization was unsteady for a significant part of its lifetime. Tong and Sirignano [3] proposed analytical solutions for diffusion and circulation in a vaporizing droplet by utilizing simplified governing equations and series solution. Rangel and Fernandez-Pello [4] solved the coupled gas and liquid phase analyses by a series expansion approach and showed that the internal

circulation had only a moderate influence in enhancing the vaporization rate of the droplet. But this result was only limited to the isothermal droplets. The above simplified models had limited accuracy because they neglected the recirculating wake near the rear stagnation point and the pressure drag cannot be obtained under the potential flow assumption in the outer region.

More accurate consideration of forced convection of the gas phase and the resulting internal circulation in the liquid phase requires the numerical solution of the complete set of Navier–Stokes, energy and species equations, combined with appropriate boundary conditions. For a single droplet with axi-symmetric inlet conditions, axi-symmetry can be assumed and the calculation is two-dimensional. Chiang et al. [5] numerically examined the transient vaporization of a fuel droplet in a hot gas stream. They solved the complete set of Navier–Stokes, energy and species equations, with considerations of droplet surface regression, deceleration of the stream flow, internal circulation inside the droplet, variable properties, and non-uniform surface temperature. Their results indicated that the influence of variable properties can be significant.

Aouina and Maas [6] numerically simulated the heating, vaporization, and ignition of a cold droplet injected in a hot gas flow. The

* Corresponding author.

E-mail address: gwu1@uci.edu (G. Wu).

Nomenclature

Latin Letters

B_h	Spalding transfer number
C_D	drag coefficient
C_i	the concentration of i th species
c_p	constant pressure specific heat
d	droplet diameter
D	diffusion coefficient
Da	Damkohler number
E_a	activation energy
h	specific thermal enthalpy
L	latent heat of vaporization
M	molecular weight
p	pressure
Pr	Prandtl number
q_k	heat of reaction for the k th global reaction
r	radial coordinate
R	droplet radius
Re	Reynolds number
R_u	universal gas constant
t	time
T	temperature
T_b	boiling temperature
T_c	critical temperature
u	velocity
U_d	velocity of the droplet
U'_∞	relative velocity between the stream and the droplet
We	Weber number

Y mass fraction

Greek Letters

θ	angular coordinate
ξ	normalized radial coordinate in the liquid phase
ρ	density
α	thermal diffusivity
λ	thermal conductivity
μ	kinetic viscosity
σ	surface tension
γ	the ratio of C_{OH} and C_H
η	catalytic efficiency
$\dot{\omega}_k$	chemical reaction rate for the k th global reaction

Subscripts

∞	ambient value
0	initial value
F	fuel vapor
g	gas phase
i	the i th species
l	liquid phase
s	surface value

Superscript

bar	dimensionless quantities
o	reference value

time and position of ignition and the 2-D gas-phase contours until and during the time of ignition were investigated. Dwyer et al. [7,8] studied the influence of surface tension on the burning of a convective methanol droplet, and concluded that the surface tension forces caused by surface mass-fraction gradients of water were important. Raghavan et al. [9] made experimental and numerical investigations of convective droplet burning. The stream velocity and droplet radius were kept constant and the interior of the droplet was not modeled. The equilibrium flame shapes and burning rates were studied for various stream velocities and droplet radius. Wu and Sirignano [10] extended their work with considerations of transient heating of the droplet, droplet surface regression, deceleration due to the drag of the droplet, internal circulation inside the droplet, and the effect of surface tension. They found that the flame had always the tendency of wake-to-envelope transition for the decelerating relative stream velocity. Pope et al. also made numerical studies of steady-state combustion [11] and some of the transient behaviors [12] for an isolated convecting burning heptane droplet. A more complete review of droplet vaporization and burning is given by Sirignano [13].

Reduced chemical mechanisms can be obtained by applying partial equilibrium and steady-state assumption to a full chemical-kinetic mechanism. None of the preceding studies employed detailed chemical kinetics for the gas-phase combustion. There are too many steps in the chemistry of liquid fuels for complete account of the elementary chemistry to be included in numerical work. The essence of the detailed chemistry, however, often can be retained in a manageable way through systematic reduction. The resulting reduced mechanisms may be anticipated to be closer to reality than the one-step empirical approximations employed previously. Such reduced chemistry for hydrocarbon diffusion flames was first developed about 20 years ago [14,15]. Peters [16] made numerical calculations and sensitivity analysis of the chemistry for methane-air flames, based on which they derived a

four-step reduced mechanism with explicit equations for steady state species. They concluded that the range of application of reduced mechanisms for flames covers a large range of stoichiometry and pressures, although they might not be applied to ignition problems where different elementary reactions are important. Card [17] obtained a four-step reduced mechanism for n-heptane from a minimal chemical-kinetic description, and used it to analyze the extinction characteristics of a single n-heptane droplet burning under quasi-steady and spherically symmetrical conditions. Reduced chemical mechanisms may not give good predictions of ignition and pollutants because some relevant radicals are assumed steady. In these cases detailed chemistry was usually used [18–20].

The objective of this study is to investigate numerically the transient burning of an n-octane fuel droplet in a hot gas stream using a four-step reduced mechanism, with considerations of droplet surface regression, deceleration of the stream flow due to the drag of the droplet, internal circulation inside the droplet, variable properties, non-uniform surface temperature, and the effect of surface tension. We extend our previous work [10] by employing a four-step reduced chemical mechanism, to study the differences in the results introduced from the improved chemical kinetics. The transient flame shape, surface temperature, and burning rates will be studied for different initial and ambient parameters. Particularly, the critical initial Damkohler number (for the determination of an initial envelope or wake flame) under various ambient conditions will be determined. The major objective of this work is to examine the effect of a four-step chemistry model, and also to study the effect of ambient conditions, which was not discussed in our previous paper [10] using one-step chemistry.

2. Problem formulation

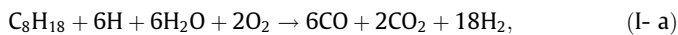
A cold droplet composed of single species of n-octane fuel is injected into a hot gas stream. That stream is an oxygen–nitrogen

mixture with velocity U_∞ , pressure p_∞ , temperature T_∞ , and mass fraction for oxygen $Y_{O_2,\infty}$. The temperature inside the droplet is initially uniform and low. As the droplet is injected into the hot stream, it is heated and is increasingly vaporized, and then ignited and burned. Internal circulation can be caused within the droplet because of the shear stress at the gas-side droplet surface and the non-uniform distribution of surface tension around the liquid-side droplet surface. The droplet has a velocity U_d . We treat a stationary droplet by having a frame of reference that instantaneously moves with that droplet velocity. A relative free stream velocity $U'_\infty = U_\infty - U_d$ is thus applied at the inflow boundary during the simulation. As the droplet is slowed down by the drag, the relative stream velocity is updated accordingly. The radius of the droplet must also be updated with time because of droplet surface regression due to the vaporization.

The following assumptions are made: (1) the Mach number is much less than unity and the dissipation terms are neglected; (2) there is no natural convection and other gravity effects; (3) the droplets remain spherical; (4) the gas mixture is an ideal gas; (5) the liquid-phase properties variation is neglected; and (6) the radiation is neglected.

Card [17] listed 32 steps as a chemical kinetic mechanism for the burning of n-heptane, which include two types of overall steps for decomposition of the alkyl radical, namely one producing C_3H_6 , the propene route, and one producing C_2H_4 , the ethylene route; and he selected the propene route (steps 1–25) to determine the reduced chemistry. For the burning of n-octane, steps 1–22 stay the same but steps 23–25 are changed from n-heptane decomposition into n-octane decomposition, as shown in Table 1. Step 25 is the reaction for C_8H_{17} decomposition and produces C_2H_4 as well as C_3H_6 ; so elements of both propene and ethylene routes are retained. This requires including steps 27–32 for C_2H_4 reactions in [17] in the main chain, but there are two possible choices for C_2H_3 reaction: step 29 (named mechanism a) or step 30 (named mechanism b). To achieve a range of possibilities for the unknown exact extent of radical removal by fuel consumption, calculations are performed with both mechanisms a and b.

Following the methodology of Peters [16], the concentrations of C_8H_{17} , C_3H_6 , CH_3CHO , CH_3O , CH_2O , HCO , CH_3 , C_2H_4 , C_2H_3 , C_2H_2 , CH_2 , HO_2 , O , and OH are eliminated by assuming these species to be in steady state and the starting mechanisms can be reduced into a four-step mechanism (with mechanism a and mechanism b only different in the first step):



The global reaction rates can be expressed in terms of the elementary reaction rates ω_j

$$\omega_I = \omega_{23} + \omega_{24},$$

$$\omega_{II} = \omega_{11f} - \omega_{11b},$$

$$\omega_{III} = \omega_5 + \omega_6 + \omega_7 + \omega_{16} - \omega_{18} + \omega_{19} + \omega_{30} \text{ for mechanism a,} \\ \text{or } \omega_5 + \omega_6 + \omega_7 + \omega_{16} - \omega_{18} + \omega_{19} - \omega_{29} \text{ for mechanism b,}$$

$$\omega_{IV} = \omega_{1f} - \omega_{1b} + \omega_8 + \omega_{18}. \quad (1)$$

As indicated in [17], ω_{19} is small compared with ω_{18} and will be neglected in the present calculation.

The concentrations of the intermediate species that appear in the global rate expressions above include C_{OH} , C_{HO_2} , C_{HCO} , C_O , C_{CH_3} , and $C_{C_2H_3}$. They need to be expressed in terms of concentrations of the seven nonsteady-state species. The concentration of OH is determined from a truncated form of steady-state relation for C_{OH} [16]: $C_{OH} = \frac{k_{3b}C_{H_2O}C_H + k_{1f}C_H C_{CO_2}}{k_{3f}C_{H_2} + k_{1b}k_{4f}k_{3b}C_{H_2}^2 / (k_{4b}k_{3f}C_{H_2}^2)}$. The concentrations of

other steady-state species can also be obtained from their steady-state relations (with the same approximations made in [17]):

$$C_{HO_2} = \frac{k_6 C_M C_{CO_2}}{k_8 + k_9 + k_{10} \gamma}, \quad C_{HCO} = \frac{3k_{23} C_F C_H}{k_{16} C_H + k_{17} C_M}, \quad C_O = \frac{k_{1f} C_{CO_2} C_H + \gamma k_{2b} C_{H_2}^2}{\gamma k_{1b} C_H + k_{2f} C_{H_2}}, \quad C_{C_2H_3} =$$

$$\frac{2k_{23} C_F C_H}{k_{29} C_M + k_{30} C_H}, \quad \text{and } C_{CH_3} = \frac{3k_{23} C_F C_H (\gamma k_{1b} C_H + k_{2f} C_{H_2})}{k_{2f} k_{18} C_{H_2} C_{CO_2} + k_{1f} k_{12} C_{CO_2} C_H + \gamma k_{12} k_{2b} C_{H_2}^2}, \quad \text{in which } \gamma =$$

C_{OH}/C_H , $k'_{2f} = k_{2f} + \gamma k_{3f} k_{4b}/k_{3b}$, $k'_{2b} = k_{2b} + \gamma k_{4f}$, $k'_{12} = k_{12} + \gamma k_{18} k_{1b}/k_{1f}$, and $k'_{23} = k_{23} + \gamma k_{24}$. The catalytic efficiency η_i ($i = N_2$, CO_2 , or H_2O) is used to express the concentration of the third body C_M as $C_M = \frac{pM_{avg}}{R_u T} \sum_i \frac{\eta_i Y_i}{M_i}$; the efficiencies of N_2 , CO_2 , and H_2O are taken to be 0.4, 1.5, and 6.5, respectively [21], with O_2 assumed the same efficiency as N_2 .

The variables have been non-dimensionalized and are listed

as follows: $\bar{r} = \frac{r}{d_0}$, $\bar{t} = \frac{t U'_{\infty,0}}{d_0}$, $\bar{u}_r = \frac{u_r}{U'_{\infty,0}}$, $\bar{u}_\theta = \frac{u_\theta}{U'_{\infty,0}}$, $\bar{p} = \frac{p}{\rho_\infty U'^2_{\infty,0}}$, $\bar{\rho} = \frac{\rho}{\rho_\infty}$,

$\bar{h} = \frac{h}{c_{p,\infty}(T_\infty - T_{s,0})}$, $\bar{T} = \frac{T - T_{s,0}}{T_\infty - T_{s,0}}$, $\bar{M}_i = \frac{M_i}{M_F}$, $\bar{c}_p = \frac{c_p}{c_{p,\infty}}$, $\bar{\mu} = \frac{\mu}{\mu_\infty}$, $\bar{\lambda} = \frac{\lambda}{\lambda_\infty}$, $\bar{\alpha} = \frac{\alpha}{\alpha_\infty}$,

$\bar{D}_i = \frac{D_i}{D_{i,\infty}}$, $\bar{\omega}_k = \frac{\omega_k}{\omega^0}$, $\bar{\sigma} = \frac{\sigma}{\sigma_0}$, where d_0 , $U'_{\infty,0}$, ω^0 and σ (or σ_0) denote

the initial droplet diameter, initial relative stream velocity, chemical reaction rate for the k th global reaction ($k = I-IV$), and surface tension (or the initial value), respectively. ω^0 is the reference rate for the overall one-step chemical reaction using values given by Westbrook and Dryer [22]. There are certain dimensionless numbers generated: initial Reynolds number $Re_0 = \frac{\rho_\infty U'_{\infty,0} d_0}{\mu_\infty}$, Prandtl number $Pr_\infty = \frac{\mu_\infty}{\rho_\infty \alpha_\infty}$, Schmidt number $Sc_{i,\infty} = \frac{\mu_\infty}{\rho_\infty D_{i,\infty}}$, Spalding transfer number $B_h = \frac{c_{p,\infty}(T_\infty - T_{s,0})}{L}$, initial Weber number $We_0 = \frac{\rho_\infty U'^2_{\infty,0} d_0}{\sigma_0}$,

and initial Damkohler number $Da_0 = \frac{d_0 U'_{\infty,0}}{\rho_\infty Y_F^0 / (\omega^0 M_F)}$ (where Y_F^0 is the reference mass fraction for the fuel vapor). The same definition of initial Damkohler number is used for both the one-step and four-step mechanisms.

The gas-phase continuity, momentum, energy and species equations and liquid-phase continuity, momentum and energy equations are coupled and solved simultaneously. There are totally $N = 8$ unsteady species including the fuel vapor, oxygen, water vapor, carbon dioxide, hydrogen, carbon monoxide, hydrogen atom, and nitrogen considered in the calculation. The species equations are applied to the first seven species, while the concentration of

Table 1

Starting mechanisms (steps 23–25, 29, and 30) and associated rate constants $k_j = A_j T^{\eta_j} \exp(-E_{a,j}/(R_u T))$, with units moles, cm, s, K, and J/mol. Other steps unlisted here (1–22, 27–28, and 31–32) are identical to those in Card [17].

Number	Reaction	A_j	η_j	$E_{a,j}$
23	$C_8H_{18} + H \rightarrow C_8H_{17} + H_2$	7.1×10^{14}	0.0	35,300
24	$C_8H_{18} + OH \rightarrow C_8H_{17} + H_2O$	2.0×10^{13}	0.0	3900
25	$C_8H_{17} \rightarrow CH_3 + 2C_2H_4 + C_3H_6$		Rate constants not used	
29	$C_2H_3 + M \rightarrow C_2H_2 + H + M$	3.0×10^{15}	0.0	134,000
30	$C_2H_3 + H \rightarrow C_2H_2 + H_2$	2.0×10^{13}	0.0	0

nitrogen is obtained from the relation that the mass fraction for all the species sums to unity. As the problem is axisymmetric, we use 2-D spherical coordinates for both gas-phase and liquid-phase computational domains. The following are the governing equations for both gas and liquid phases.

Continuity equation:

$$\frac{\partial \bar{\rho}}{\partial \bar{t}} + \frac{1}{\bar{r}^2 \sin \theta} \left[\frac{\partial (\bar{r}^2 \sin \theta \bar{\rho} \bar{u}_r)}{\partial \bar{r}} + \frac{\partial (\bar{r} \sin \theta \bar{\rho} \bar{u}_\theta)}{\partial \theta} \right] = 0. \quad (2)$$

Momentum equation in r -direction:

$$\begin{aligned} \frac{\partial (\bar{\rho} \bar{u}_r)}{\partial \bar{t}} + \frac{1}{\bar{r}^2 \sin \theta} \left[\frac{\partial (\bar{r}^2 \sin \theta \bar{\rho} \bar{u}_r \bar{u}_r)}{\partial \bar{r}} + \frac{\partial (\bar{r} \sin \theta \bar{\rho} \bar{u}_\theta \bar{u}_r)}{\partial \theta} \right] - \frac{\bar{\rho} \bar{u}_\theta^2}{\bar{r}} \\ = - \frac{\partial \bar{p}}{\partial \bar{r}} - \frac{1}{Re_0} \left[\frac{1}{\bar{r}^2} \frac{\partial}{\partial \bar{r}} (\bar{r}^2 \bar{\tau}_{rr}) + \frac{1}{\bar{r} \sin \theta} \frac{\partial}{\partial \theta} (\bar{\tau}_{r\theta} \sin \theta) - \frac{\bar{\tau}_{\theta\theta} + \bar{\tau}_{\phi\phi}}{\bar{r}} \right]. \end{aligned} \quad (3)$$

Momentum equation in θ -direction:

$$\begin{aligned} \frac{\partial (\bar{\rho} \bar{u}_\theta)}{\partial \bar{t}} + \frac{1}{\bar{r}^2 \sin \theta} \left[\frac{\partial (\bar{r}^2 \sin \theta \bar{\rho} \bar{u}_r \bar{u}_\theta)}{\partial \bar{r}} + \frac{\partial (\bar{r} \sin \theta \bar{\rho} \bar{u}_\theta \bar{u}_\theta)}{\partial \theta} \right] + \frac{\bar{\rho} \bar{u}_r \bar{u}_\theta}{\bar{r}} \\ = - \frac{1}{\bar{r}} \frac{\partial \bar{p}}{\partial \theta} \\ - \frac{1}{Re_0} \left[\frac{1}{\bar{r}^2} \frac{\partial}{\partial \bar{r}} (\bar{r}^2 \bar{\tau}_{r\theta}) + \frac{1}{\bar{r} \sin \theta} \frac{\partial}{\partial \theta} (\bar{\tau}_{\theta\theta} \sin \theta) + \frac{\bar{\tau}_{r\theta} - \bar{\tau}_{\phi\phi} \cot \theta}{\bar{r}} \right]. \end{aligned} \quad (4)$$

The components of the shear stress tensor in axi-symmetric spherical coordinates (normalized by $\frac{\mu_\infty U'_{\infty,0}}{d_0}$) are used in the momentum equations, with $\bar{\tau}_{rr} = -\bar{\mu} \left[2 \frac{\partial \bar{u}_r}{\partial \bar{r}} - \frac{2}{3} (\nabla \cdot \bar{u}) \right]$, $\bar{\tau}_{\theta\theta} = -\bar{\mu} \left[2 \left(\frac{1}{\bar{r}} \frac{\partial \bar{u}_\theta}{\partial \theta} + \frac{\bar{u}_r}{\bar{r}} \right) - \frac{2}{3} (\nabla \cdot \bar{u}) \right]$, $\bar{\tau}_{\phi\phi} = -\bar{\mu} \left[2 \left(\frac{\bar{u}_r}{\bar{r}} + \frac{\bar{u}_\theta \cot \theta}{\bar{r}} \right) - \frac{2}{3} (\nabla \cdot \bar{u}) \right]$, and $\bar{\tau}_{r\theta} = -\bar{\mu} \left[\bar{r} \frac{\partial}{\partial \bar{r}} \left(\frac{\bar{u}_\theta}{\bar{r}} \right) + \frac{\partial \bar{u}_r}{\partial \theta} \right]$.

Energy equation:

$$\begin{aligned} \frac{\partial (\bar{\rho} \bar{h})}{\partial \bar{t}} + \frac{1}{\bar{r}^2 \sin \theta} \left[\frac{\partial (\bar{r}^2 \sin \theta \bar{\rho} \bar{u}_r \bar{h})}{\partial \bar{r}} + \frac{\partial (\bar{r} \sin \theta \bar{\rho} \bar{u}_\theta \bar{h})}{\partial \theta} \right] \\ = \frac{1}{Re_0 Pr_\infty \bar{r}^2 \sin \theta} \left[\frac{\partial}{\partial \bar{r}} \left(\bar{\rho} \bar{\alpha} \bar{r}^2 \sin \theta \frac{\partial \bar{h}}{\partial \bar{r}} \right) + \frac{\partial}{\partial \theta} \left(\bar{\rho} \bar{\alpha} \sin \theta \frac{\partial \bar{h}}{\partial \theta} \right) \right] \\ + S_h, \end{aligned} \quad (5)$$

in which $S_h = \nabla \cdot (\sum_{i=1}^N \bar{\rho} \bar{D}_i \bar{h}_i \nabla Y_i) / (Re_0 Sc_{i,\infty}) - \nabla \cdot (\bar{\rho} \bar{\alpha} \sum_{i=1}^N \bar{h}_i \nabla Y_i) / (Re_0 Pr_\infty) + \frac{Y_F^0 Da_0 \sum_{k=1}^{N_V} q_k \bar{\omega}_k}{M_F c_{p,\infty} (T_\infty - T_{s,0})}$ for the gas phase, and $S_h = 0$ for the liquid phase. Da_0 is the initial Damkohler number. q_k and $\bar{\omega}_k$ are the heat of reaction and normalized chemical reaction rate ($\bar{\omega}_k / \dot{\omega}^0$) for the k th global reaction. The reference rate of the overall chemical reaction $\dot{\omega}^0$ is defined as the chemical reaction rate for the one-step mechanism $\dot{\omega} = A \exp(-E_a / (R_u T)) [Fuel]^a [Oxidizer]^b \frac{\text{mol}}{\text{cm}^3 \text{s}}$ [22], at the reference conditions of T_∞ , ρ_∞ , $Y_{O_2,\infty}$, and the stoichiometric mass fraction for the fuel vapor Y_F^0 . The values of $\dot{\omega}^0$ and the initial Damkohler number Da_0 will be very sensitive to the choice of the reference temperature, and T_∞ is a good choice for cases of high ambient temperature where autoignition becomes possible. The temperature is obtained from the enthalpy.

Gas-phase species equation:

$$\begin{aligned} \frac{\partial (\bar{\rho} Y_i)}{\partial \bar{t}} + \frac{1}{\bar{r}^2 \sin \theta} \left[\frac{\partial (\bar{r}^2 \sin \theta \bar{\rho} \bar{u}_r Y_i)}{\partial \bar{r}} + \frac{\partial (\bar{r} \sin \theta \bar{\rho} \bar{u}_\theta Y_i)}{\partial \theta} \right] \\ = \frac{1}{Re_0 Sc_{i,\infty} \bar{r}^2 \sin \theta} \left[\frac{\partial}{\partial \bar{r}} \left(\bar{\rho} \bar{D}_i \bar{r}^2 \sin \theta \frac{\partial Y_i}{\partial \bar{r}} \right) + \frac{\partial}{\partial \theta} \left(\bar{\rho} \bar{D}_i \sin \theta \frac{\partial Y_i}{\partial \theta} \right) \right] \\ + \bar{\omega}_i \bar{M}_i Y_F^0 Da_0, \end{aligned} \quad (6)$$

in which \bar{M}_i and $\bar{\omega}_i$ are the normalized molecular weight and rate of production (+) or consumption (−) for the i th species. The following relations can be obtained for $\dot{\omega}_i$ from the stoichiometry of the four

global reactions: $\dot{\omega}_F = -\dot{\omega}_I$, $\dot{\omega}_{O_2} = -2\dot{\omega}_I - \dot{\omega}_{IV}$, $\dot{\omega}_{H_2O} = -6\dot{\omega}_I - \dot{\omega}_{II} + 2\dot{\omega}_{IV}$, $\dot{\omega}_{CO_2} = 2\dot{\omega}_I + \dot{\omega}_{II}$, $\dot{\omega}_{H_2} = 18\dot{\omega}_I + \dot{\omega}_{II} + \dot{\omega}_{III} - 3\dot{\omega}_{IV}$ for mechanism a or $20\dot{\omega}_I + \dot{\omega}_{II} + \dot{\omega}_{III} - 3\dot{\omega}_{IV}$ for mechanism b, $\dot{\omega}_{CO} = 6\dot{\omega}_I - \dot{\omega}_{II}$, and $\dot{\omega}_H = -6\dot{\omega}_I - 2\dot{\omega}_{III} + 2\dot{\omega}_{IV}$ for mechanism a or $-10\dot{\omega}_I - 2\dot{\omega}_{III} + 2\dot{\omega}_{IV}$ for mechanism b. The chemistry is started with an initial hydrogen-atom mass fraction of 10^{-6} because for the four-step chemistry modeling the ignition cannot occur automatically without an artificial supply of the H atom. The four-step reduced chemistry does not give desirable predictions of the instant and location of the ignition, because the OH radical is assumed a steady-state species and not tracked. Furthermore, the instant and location of the ignition are influenced by the location and concentration of H atom which is artificially applied for the ignition. Therefore, the quantitative discussion of the ignition is not suitable for the four-step chemistry and thus not included in the current study, which is focused on the burning behavior because the reduced chemistry employed is inappropriate for ignition, excluding, for example, the low-temperature chemistry that strongly influences ignition under certain conditions.

The droplet surface regresses during vaporization, and the droplet radius is a function of time. Therefore, the liquid-phase domain shrinks while the gas-phase domain expands. To consider this, the adjustments of radial coordinate or mesh are needed. Details are provided in Wu and Sirignano [10].

Assuming the gas flow is coming from left to right (Fig. 1), the left half circle of the gas-phase outer boundary is regarded as the inlet boundary, and the right half circle of the gas-phase outer boundary is regarded as the outlet boundary. Boundary conditions at the droplet surface need to be specified for both gas and liquid phase based on balance of force, and heat and mass transfer. The boundaries of $\theta = 0$ and $\theta = \pi$ are axis of symmetry where symmetry boundary conditions can be applied.

Boundary conditions at the inlet:

$$\begin{aligned} \bar{u}_r = -\bar{U}'_\infty \cos \theta, \bar{u}_\theta = \bar{U}'_\infty \sin \theta, \bar{T} = 1, \\ Y_i = Y_{O_2,\infty} \text{ for } O_2 \text{ and } 0 \text{ for others.} \end{aligned} \quad (7)$$

Boundary conditions at the outlet:

$$\frac{D\bar{u}_r}{D\bar{t}} = \frac{D\bar{u}_\theta}{D\bar{t}} = \frac{D\bar{T}}{D\bar{t}} = \frac{DY_i}{D\bar{t}} = 0. \quad (8)$$

Boundary conditions at the droplet surface:

Conservation of mass flux:

$$\begin{aligned} \bar{u}_{g,r,s} = - \frac{1}{Re_0 Sc_{F,\infty}} \frac{\bar{D}_F (\partial Y_F / \partial \bar{r})_s}{1 - Y_{F,s}}, \\ \bar{\rho}_g \left(\bar{u}_{g,r,s} - \frac{d\bar{R}}{d\bar{t}} \right) = \bar{\rho}_l \left(\bar{u}_{l,r,s} - \frac{d\bar{R}}{d\bar{t}} \right), \\ \frac{d\bar{R}}{d\bar{t}} = - \frac{\bar{\rho}_g}{\bar{\rho}_l} \bar{u}_{g,r,s}. \end{aligned} \quad (9)$$

Continuity of tangential velocity and shear stress in θ direction:

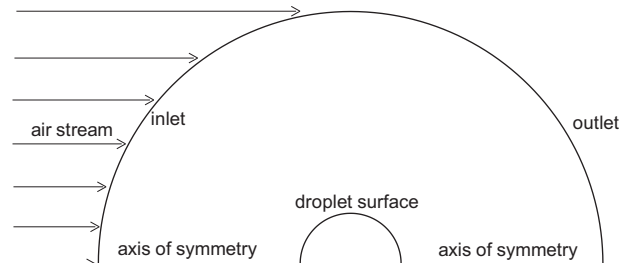


Fig. 1. A sketch of the computational domains and boundaries.

$$\begin{aligned} \bar{u}_{g,\theta,s} &= \bar{u}_{l,\theta,s}, \\ \bar{\mu}_g \left(\frac{\partial \bar{u}_{g,\theta}}{\partial \bar{r}} - \frac{\bar{u}_{g,\theta}}{\bar{R}} + \frac{1}{\bar{R}} \frac{\partial \bar{u}_{g,r}}{\partial \theta} \right)_s &+ \frac{1}{\bar{R}} \frac{Re_0}{We_0} \left(\frac{\partial \bar{\sigma}}{\partial \theta} \right)_s \\ &= \bar{\mu}_l \left(\frac{\partial \bar{u}_{l,\theta}}{\partial \bar{r}} - \frac{\bar{u}_{l,\theta}}{\bar{R}} + \frac{1}{\bar{R}} \frac{\partial \bar{u}_{l,r}}{\partial \theta} \right)_s, \end{aligned} \quad (10)$$

where We_0 is the initial Weber number, $\bar{\sigma}$ is the normalized surface tension which is given by

$$\bar{\sigma} = A \left(1 - \frac{T_s}{T_c} \right)^n / \sigma_0. \quad (11)$$

A , T_c , and n are coefficients for liquid fuel, and σ_0 is the initial value.

Continuity of surface temperature and balance of energy flux:

$$\begin{aligned} \bar{T}_{g,s} &= \bar{T}_{l,s}, \\ \bar{\lambda}_g \left(\frac{\partial \bar{T}_g}{\partial \bar{r}} \right)_s &= \bar{\lambda}_l \left(\frac{\partial \bar{T}_l}{\partial \bar{r}} \right)_s + \bar{\rho}_g \bar{u}_{g,r,s} \frac{Re_0 Pr_\infty}{B_h}. \end{aligned} \quad (12)$$

The mass fraction of the fuel vapor is given by

$$Y_{F,s} = \frac{\frac{M_F}{M_A}}{\exp \left(\frac{LM_F}{R_u} \left(\frac{1}{T_{g,s}} - \frac{1}{T_b} \right) \right) + \frac{M_F}{M_A} - 1}, \quad (13)$$

where M_A is the average molecular weight of the gas mixture (without the fuel vapor) at the droplet surface. This is derived from the Clausius–Clapeyron relation and the relation that the mole fractions for the fuel vapor and other species sum to unity.

For the non-vaporizing species, there is no net mass flux for each species, i.e.,

$$\left(-\bar{\rho} \bar{D}_i \frac{\partial Y_i}{\partial \bar{r}} + Re_0 Sc_{i,\infty} \bar{\rho} \bar{u}_{g,r,s} Y_i \right)_s = 0. \quad (14)$$

Boundary conditions at the axis of symmetry:

$$\bar{u}_\theta = \frac{\partial \bar{u}_r}{\partial \theta} = \frac{\partial \bar{T}}{\partial \theta} = \frac{\partial Y_i}{\partial \theta} = 0. \quad (15)$$

The droplet is slowed down by the drag in the transient process. There are three types of drag: pressure drag, friction drag and thrust drag [10], and the total drag C_D is a sum of the three types of drag. The instantaneous velocity of the droplet or the relative stream velocity is determined by

$$\frac{d\bar{U}_d}{dt} = -\frac{d\bar{U}'_\infty}{dt} = \frac{3}{8} \frac{1}{\bar{\rho}_l} \frac{\bar{U}'_\infty{}^2}{\bar{R}} C_D. \quad (16)$$

3. Solution procedure

We consider a droplet composed of pure n-octane; so, the effect of different fuel types is not examined. The thermodynamic and transport properties for the gas mixture are calculated by polynomials and semi-empirical equations [23–25]. The momentum equations, enthalpy equation and species equations (gas phase only) are solved in order for each domain. Then the temperature distributions are obtained by solving the differential form of $h = h(T, Y_i)$. The droplet radius and relative velocity between the droplet and the stream are updated instantaneously after each time step.

The Semi-Implicit Method for Pressure Linked Equations (SIMPLE) is used to solve the coupled Navier–Stokes, energy and species equations for both gas and liquid phase. Staggered grids are used with three different control volumes for the two components of velocity and pressure correction (temperature, mass fraction or scalar properties) respectively. Forward time and hybrid scheme are applied in the discretization. For the iterations at each time step, Tri-Diagonal Matrix Algorithm (TDMA) is used to solve over

nodes in each row along the θ direction, and it sweeps forward and backward in the r direction. The grid and time-step independence have been tested, and the following selection for the size of mesh and time step is found to give a good balance between solution accuracy and computational economy. The mesh in the θ direction is uniform with $\Delta\theta = \pi/180$ for both liquid and gas phase. The mesh in the r direction is uniform for the liquid phase with $\Delta r = 0.01R$. For the gas phase, the mesh in the r direction is uniform ($\Delta r = 0.01R_0$) within a layer with a thickness of $0.5R_0$ from the initial droplet surface, but diverges with a factor of 1.1 with distance away from this layer. As the droplet surface regresses, the new cells added to the gas phase always have a mesh size of $\Delta r = 0.01R_0$. Because the characteristic chemical time for some global reaction step in this study is smaller than the characteristic chemical time for overall one-step reaction in [10], the time step size needs to be smaller in this study. The time step is still fixed and it takes about 10^6 time steps for 99% of the droplet volume to be vaporized. Each calculation requires about 48 h of time on the Pentium based computers. The errors due to the mesh-update scheme in the gas phase are found to be small, and have negligible influence on the stability of the calculations.

4. Results and discussion

4.1. Comparisons with the one-step kinetics

In this section, the transient behaviors of both mechanism a and mechanism b of the four-step reduced mechanism are studied and then compared with the results of the one-step kinetics. The initial droplet radius is $R_0 = 25 \mu\text{m}$. The ambient conditions are: $p_\infty = 20 \text{ atm}$, $T_\infty = 1500 \text{ K}$, and $Y_{O_2,\infty} = 0.233$, if not mentioned otherwise. The initial relative stream velocity $U'_{\infty,0}$ varies for different cases, resulting in different initial Reynolds number Re_0 and initial Damkohler number Da_0 .

Various cases are studied for mechanism a and mechanism b of the four-step reduced mechanism. From the comparisons of the transient burning behaviors, it is found that the differences between mechanism a and mechanism b are very small and can thus be neglected. In the fuel-consumption step (step I) mechanism b consumes 10 moles of H atom per mole of fuel vapor while mechanism a consumes only 6 moles of H atom per mole of fuel vapor; however, the rate of H-atom recombination (step III) for mechanism b is smaller than that for mechanism a by a value of $\omega_{29} + \omega_{30}$. So, the agreement of the instantaneous behaviors between mechanism a and mechanism b can be explained from the balance of the difference of H-atom stoichiometry in step I and the difference of H-atom-recombination rate in step III for the two types of four-step reduced mechanisms.

The results of the four-step reduced mechanism are compared with the one-step mechanism in Fig. 2a and b, for the instantaneous average surface temperature and normalized mass burning rate. The mass burning rate is defined based on the surface regression rate or droplet vaporization rate, which might have a minor deviation from the fuel consumption rate due to fuel accumulation in the region between droplet and flame in the unsteady process. The decreasing $(R/R_0)^{1.5}$ is used as the normalized time scale because it is asymptotically linear with time [26]. We consider three cases with different initial relative stream velocity, i.e., $Re_0 = 11, 45$, and 67 . The case with $Re_0 = 11$ has an initial envelope flame. The cases with $Re_0 = 45$ and 67 have an initial wake flame, and the wake flame will be transitioned into an envelope flame at some instant during the lifetime, which is indicated by a sharp increase in the average surface temperature. Figure 2a shows that the four-step mechanism has a sharper increase of the average surface temperature during the wake-to-envelope transition than the one-step

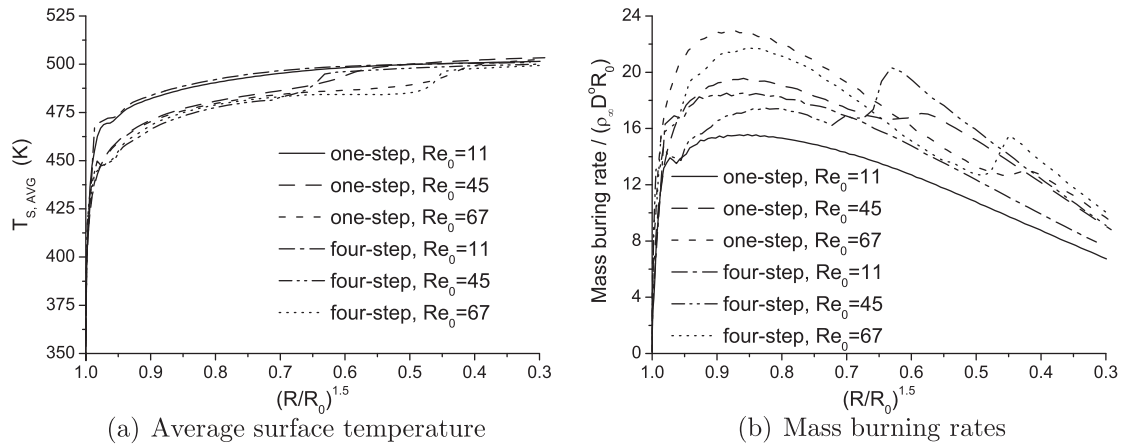


Fig. 2. The comparisons of the instantaneous quantities between the one-step mechanism and the four-step mechanism, for the cases of $Re_0 = 11, 45,$ and 67 .

mechanism; however, the instants of the wake-to-envelope transition for the two mechanisms have no major differences (for both cases of $Re_0 = 45$ and 67). Figure 2b shows that the four-step mechanism has smaller mass burning rate for a wake flame (before the wake-to-envelope transition for the cases of $Re_0 = 45$ and 67) but greater mass burning rate for an envelope flame (the case of $Re_0 = 11$, and after the wake-to-envelope transition for the cases of $Re_0 = 45$ and 67) than the one-step mechanism. So, the four-step mechanism yields greater overall mass burning rate for an initial envelope flame. However, the two mechanisms have closer overall mass burning rates for an initial wake flame because the mass burning rate for the four-step mechanism is smaller during the period with a wake flame but greater after the wake-to-envelope transition.

The results for the one-step mechanism and four-step mechanism are also compared at other ambient conditions. Figure 3a and b compare the transient average surface temperature and mass burning rate for the two mechanisms at $Re_0 = 45$ with different ambient conditions: (1) $p_\infty = 15$ atm, $T_\infty = 1500$ K and $Y_{O_2,\infty} = 0.233$; (2) $p_\infty = 20$ atm, $T_\infty = 1500$ K and $Y_{O_2,\infty} = 0.28$; (3) $p_\infty = 20$ atm, $T_\infty = 1200$ K and $Y_{O_2,\infty} = 0.233$. The two mechanisms still have no major differences in the instant of the wake-to-envelope transition at the lower ambient pressure $p_\infty = 15$ atm and greater ambient mass fraction of oxygen $Y_{O_2,\infty} = 0.28$. However, at the lower ambient temperature $T_\infty = 1200$ K, the four-step mechanism has obviously earlier wake-to-envelope transition than the one-step mechanism. For all the ambient conditions examined, the

four-step mechanism has smaller mass burning rate for a wake flame but greater mass burning rate for an envelope flame than the one-step mechanism.

From [10] using one-step kinetics, there exists a critical initial Damkohler number $Da_{0,cr}$ above which it has an initial envelope flame and below which it has an initial wake flame, and its value is 1.02 for n-octane droplet at the ambient conditions of $p_\infty = 20$ atm, $T_\infty = 1500$ K, and $Y_{O_2,\infty} = 0.233$. For the four-step reduced mechanism, the critical initial Damkohler number is found to be 0.95 for the same fuel type and ambient conditions, which has no major difference from the value using one-step kinetics. The critical initial Damkohler number varies for different ambient conditions. Table 2 lists the critical initial Damkohler numbers for both chemical mechanisms at four different ambient conditions. It shows that the two mechanisms have small differences in the critical initial Damkohler number at all the ambient conditions, although the critical initial Damkohler number for the four-step mechanism is always slightly smaller than that for the one-step mechanism. More discussion will be made on the critical initial Damkohler number at various ambient conditions for the four-step mechanism in Section 4.3.

4.2. Flow and flame behavior based upon initial and ambient parameters

In this section, the flame structure will be investigated for an envelope flame and a wake flame, and the transient behaviors will

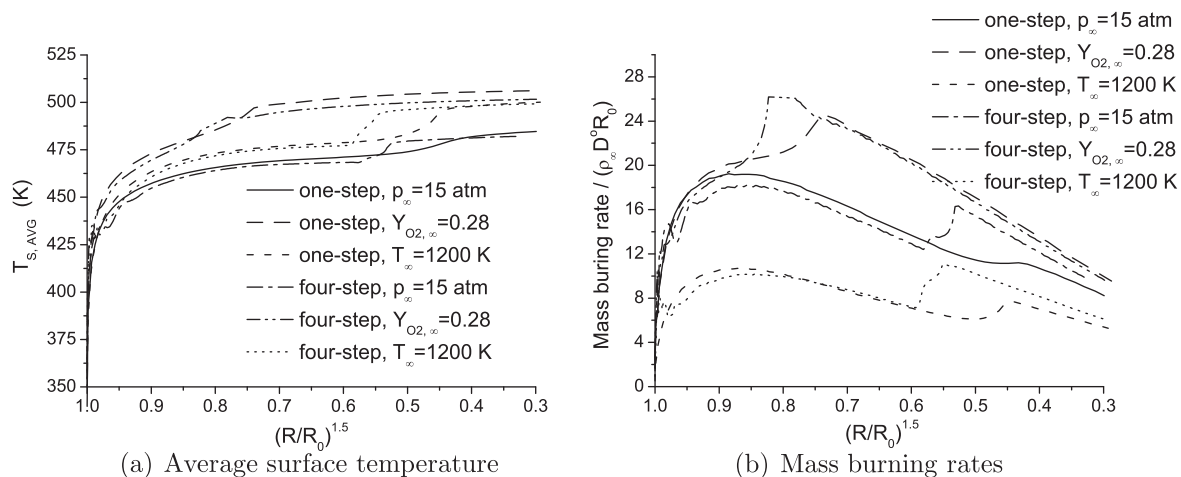


Fig. 3. The comparisons of the instantaneous quantities between the one-step mechanism and the four-step mechanism, for the cases at the same $Re_0 = 45$ and different ambient conditions: (1) $p_\infty = 15$ atm, $T_\infty = 1500$ K and $Y_{O_2,\infty} = 0.233$; (2) $p_\infty = 20$ atm, $T_\infty = 1500$ K and $Y_{O_2,\infty} = 0.28$; (3) $p_\infty = 20$ atm, $T_\infty = 1200$ K and $Y_{O_2,\infty} = 0.233$.

Table 2

The critical initial Damkohler number for bifurcations of the initial flame structure for one-step mechanism and four-step mechanism at four different ambient conditions: (a) $p_\infty = 20$ atm, $T_\infty = 1500$ K and $Y_{O_2,\infty} = 0.233$; (b) $p_\infty = 15$ atm, $T_\infty = 1500$ K and $Y_{O_2,\infty} = 0.233$; (c) $p_\infty = 20$ atm, $T_\infty = 1500$ K and $Y_{O_2,\infty} = 0.28$; (d) $p_\infty = 20$ atm, $T_\infty = 1200$ K and $Y_{O_2,\infty} = 0.233$.

	Condition a	Condition b	Condition c	Condition d
One-step	1.02	1.07	0.74	0.28
Four-step	0.95	0.98	0.69	0.23

be studied at various ambient temperature, pressure and mass fraction of oxygen. The initial droplet radius is 25 μm for the cases studied if not mentioned otherwise.

For the four-step reduced mechanism, the field of gas-phase temperature or oxygen concentration manifests the overall flame shape, while the field of the reaction rates for the four steps and concentrations of various unsteady or steady species might provide more insight for the flame structure. Figures 4 and 5 show the contours of the gas-phase temperature, the reaction rates for the four

steps, and concentrations of H atom and OH radical at an early instant during the lifetime for the cases of $Re_0 = 11$ ($Da_0 = 1.2$) and $Re_0 = 67$ ($Da_0 = 0.2$), with the same ambient conditions of $p_\infty = 20$ atm, $T_\infty = 1500$ K, and $Y_{O_2,\infty} = 0.233$. The flame is an initial envelope flame for the first case with large Da_0 and an initial wake flame for the second case with smaller Da_0 . For both envelope flame and wake flame, a region of positive peak values exists for the reaction rates for all the four steps; however, a region of negative peak values also exists only for the water-gas-shift step (step II) and the H-atom-recombination step (step III). The region of negative peak values exists for ω_{II} and ω_{III} because there are negative components in their rates which are comparable to the positive components and have peak values in a region different from that for the positive components. For the water-gas-shift step, ω_{II} is determined by $(k_{11f}C_{CO}C_{OH} - k_{11b}C_{CO_2}C_H)$, and the region with peak concentrations of H atom which contribute to the negative component is a little closer to the droplet surface than the region with peak concentrations of OH radical which contribute to the positive component.

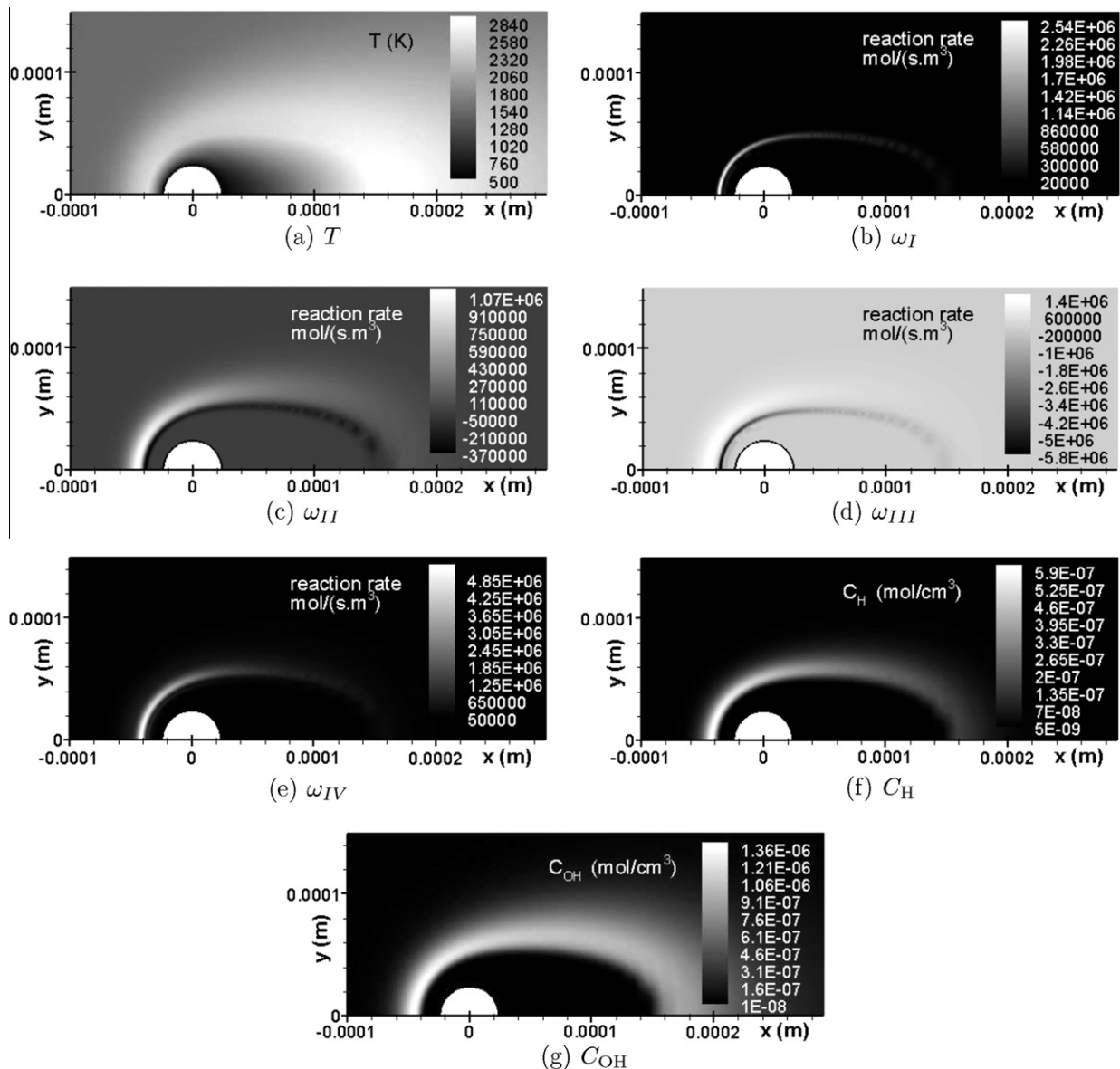


Fig. 4. The contours of the gas-phase temperature, the reaction rates for the four steps, and concentrations of H atom and OH radical at an early instant during the lifetime for the case of $Re_0 = 11$ ($Da_0 = 1.2$), with the ambient conditions of $p_\infty = 20$ atm, $T_\infty = 1500$ K, and $Y_{O_2,\infty} = 0.233$.

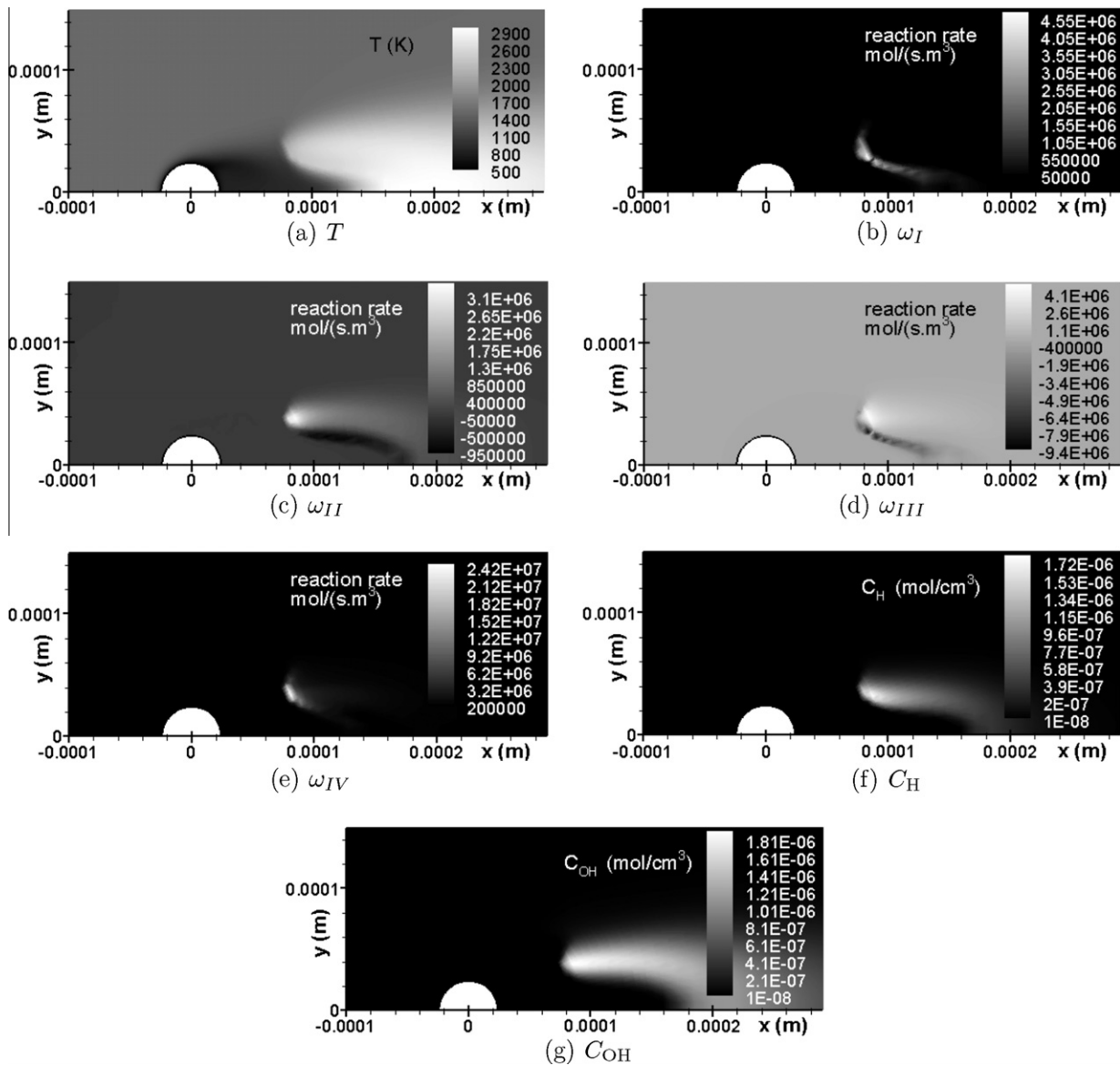


Fig. 5. The contours of the gas-phase temperature, the reaction rates for the four steps, and concentrations of H atom and OH radical at an early instant during the lifetime for the case of $Re_0 = 67$ ($Da_0 = 0.2$), with the ambient conditions of $p_\infty = 20$ atm, $T_\infty = 1500$ K, and $Y_{O_2,\infty} = 0.233$.

The cases with different ambient temperature (1200 K and 1500 K) are compared in Fig. 6, with $p_\infty = 20$ atm, $Y_{O_2,\infty} = 0.233$, and $Re_0 = 45$. The initial Damkohler number Da_0 is 0.04 for the case with $T_\infty = 1200$ K and 0.3 for the case with $T_\infty = 1500$ K. As Da_0 is the ratio of the initial residence time and the reference chemical time, the case with $T_\infty = 1200$ K has smaller Da_0 because of a much greater reference chemical time, although the initial residence time is also greater. It is obvious that the case with the lower ambient temperature has later wake-to-envelope transition and smaller mass burning rate, due to the smaller Da_0 which favors a wake flame and also the slower heating of the droplet at the lower ambient temperature.

The cases with different ambient pressure (15 atm and 20 atm) are studied at $T_\infty = 1500$ K and $Y_{O_2,\infty} = 0.233$. The instantaneous quantities are compared in Fig. 7 for three cases: $p_\infty = 20$ atm and $Re_0 = 45$ (case 1), $p_\infty = 15$ atm and $Re_0 = 45$ (case 2), and $p_\infty = 15$ atm and $Re_0 = 34$ (case 3). In comparison with case 1, case 2 has the same initial Reynolds number but smaller initial residence time, and case 3 has the same initial residence time but smaller initial Reynolds number. As lower ambient pressure yields

greater reference chemical time, the order of the initial Damkohler number for the three cases is: $Da_{0,1} > Da_{0,3} > Da_{0,2}$. Case 1 with the higher ambient pressure has greater overall mass burning rate than cases 2 and 3, because higher ambient pressure results in greater gas density and thus greater concentrations of reactants at the same molar fractions. However, higher ambient pressure also yields greater boiling point and thus smaller molar fraction of fuel vapor near the droplet surface in the early period with low surface temperature. This can explain why cases 1 and 3 with different Da_0 have no major difference in the instant of wake-to-envelope transition (note that case 2 with the smallest Da_0 still has the latest wake-to-envelope transition), and why case 2 has greater mass burning rate than case 1 for some time during the early period.

The cases with various ambient mass fraction of oxygen are studied at $p_\infty = 20$ atm and $T_\infty = 1200$ K. All the cases have the same initial Reynolds number $Re_0 = 45$. Figure 8a and b make comparisons of the instantaneous average surface temperature and normalized mass burning rate for these cases. It has an initial wake flame for the case with the ambient mass fraction of oxygen as in

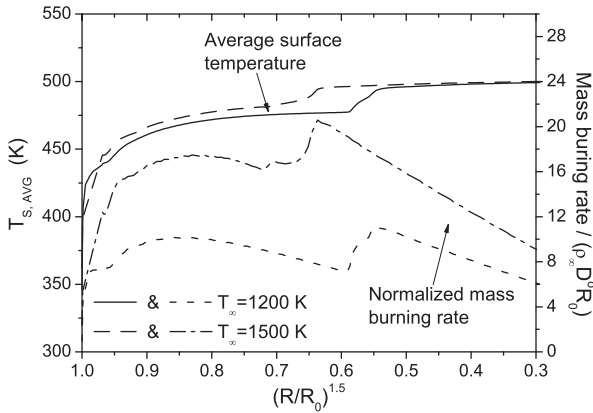


Fig. 6. The comparisons of the instantaneous average surface temperature and normalized mass burning rate between two cases with different ambient temperature (1200 K and 1500 K), with $p_\infty = 20$ atm, $Y_{O_2,\infty} = 0.233$, and $Re_0 = 45$.

the air ($Y_{O_2,\infty} = 0.233$). As the ambient mass fraction of oxygen increases, the sharp increase of the average surface temperature advances during the lifetime first and then into the initial heating and ignition period, which indicates that the instant of wake-to-envelope transition advances with increasing ambient mass fraction of oxygen, and finally the initial flame becomes an envelope flame when the ambient mass fraction of oxygen exceeds some critical value (approximately 0.5 for the current ambient pressure and

temperature). This preference for an envelope flame can be explained from the faster oxidation kinetics and greater Damkohler number for greater ambient mass fraction of oxygen. For an initial wake flame, the mass burning rate increases rapidly as the ambient mass fraction of oxygen increases. When the initial flame becomes an envelope flame, the mass burning rate still increases modestly with the increasing ambient mass fraction of oxygen, although the increase is not as fast as the cases with an initial wake flame.

4.3. Critical initial Damkohler number for the determination of the initial flame shape

For the four-step reduced mechanism, the critical initial Damkohler number for bifurcations of the initial flame structure is 0.95 for n-octane droplet at the ambient conditions of $p_\infty = 20$ atm, $T_\infty = 1500$ K, and $Y_{O_2,\infty} = 0.233$. As the ambient conditions vary, the variation in the critical initial Damkohler number is uncertain. The initial Damkohler number is simply defined as the ratio of the initial residence time and a reference chemical time determined by the ambient conditions, and the influence of the ambient conditions might be overestimated or underestimated. So, we will define a modified initial Damkohler number Da_0^m to account better for the influence of the ambient conditions. The critical initial Damkohler number can be written as a function of p_∞ , T_∞ , and $Y_{O_2,\infty}$, i.e., $Da_{0,cr} = 0.95 \left(\frac{p_\infty}{20 \text{ atm}}\right)^a \left(\frac{T_\infty}{1500 \text{ K}}\right)^b \left(\frac{Y_{O_2,\infty}}{0.233}\right)^c$, in which a, b and c are constants to be determined. We use the least-squares fitting method to determine the constants, based on the data of eleven cases with

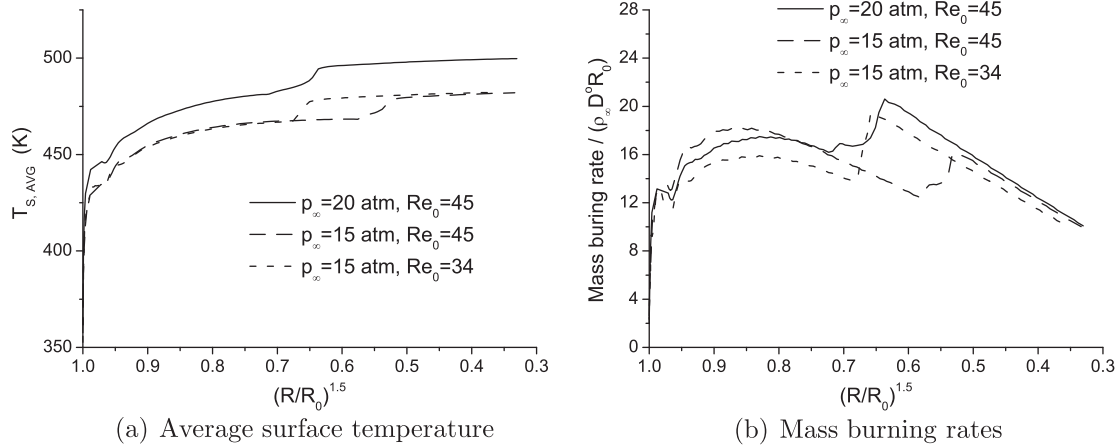


Fig. 7. The comparisons of the instantaneous quantities for the cases with different ambient pressure (15 atm and 20 atm), at the same $T_\infty = 1500$ K and $Y_{O_2,\infty} = 0.233$.

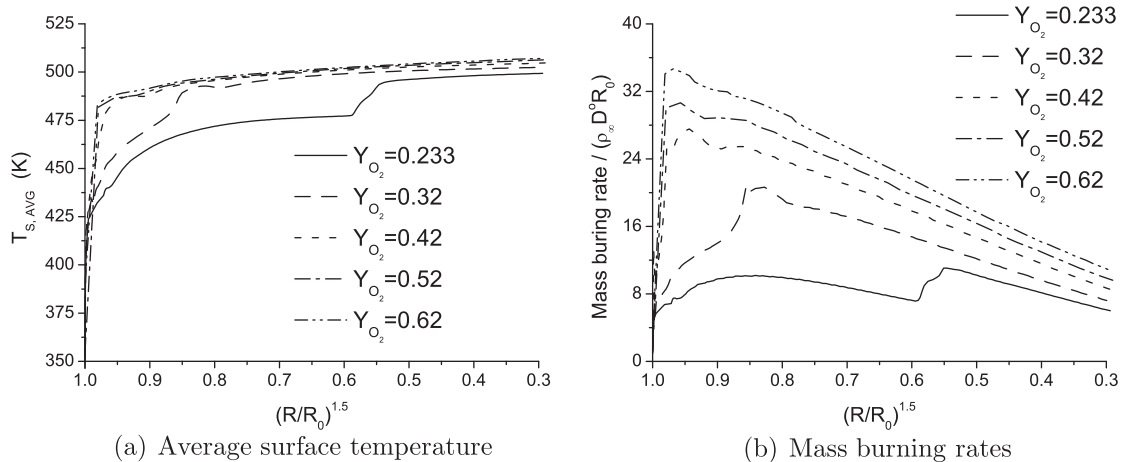


Fig. 8. The comparisons of the instantaneous quantities for the cases with different ambient mass fraction of oxygen, at the same $p_\infty = 20$ atm, $T_\infty = 1200$ K, and $Re_0 = 45$.

$p_\infty = 10, 15$ or 20 atm, $T_\infty = 1200, 1350$ or 1500 K, and $Y_{O_2,\infty} = 0.233, 0.5$ or 0.62 . The fitting results are $a = -0.07$, $b = 7.18$, and $c = -1.31$, with the standard error being $0.03, 0.41$ and 0.07 , respectively. The maximum percent deviation of $Da_{0,cr}$ from the fitting value is 17% . So, we have

$$Da_{0,cr} = 0.95 \left(\frac{p_\infty}{20 \text{ atm}} \right)^{-0.07} \left(\frac{T_\infty}{1500 \text{ K}} \right)^{7.18} \left(\frac{Y_{O_2,\infty}}{0.233} \right)^{-1.31} \quad (17)$$

If a modified initial Damkohler number is defined as

$$Da_0^m = Da_0 \left(\frac{p_\infty}{20 \text{ atm}} \right)^{0.07} \left(\frac{T_\infty}{1500 \text{ K}} \right)^{-7.18} \left(\frac{Y_{O_2,\infty}}{0.233} \right)^{1.31} \quad (18)$$

with $Da_0 = \frac{d_0/U'_{\infty,0}}{\rho_\infty Y_{F,i}^{2/(\alpha^2 M_F^2)}}$, then we will have $Da_{0,cr}^m = 0.95$, indicating that the modified initial Damkohler number has a constant critical value, regardless of the ambient conditions applied.

5. Concluding remarks

The transient burning of an n-octane fuel droplet in a hot gas stream has been analyzed using a four-step reduced mechanism, with considerations of droplet surface regression, deceleration of the stream flow, liquid motion, variable properties, non-uniform surface temperature and the consequent effect of surface tension. The transient flame shape, surface temperature, and burning rates are investigated under different initial and ambient parameters. The critical initial Damkohler number (for the determination of an initial envelope or wake flame) is determined under various ambient conditions.

There are two different mechanisms for the four-step reduced mechanism, i.e., mechanism a and mechanism b which are only different in the choice of the vinyl C_2H_3 destruction reaction. From the comparisons of the transient burning behaviors, it is found that the differences between mechanism a and mechanism b are very small and can thus be neglected.

The four-step mechanism has a sharper increase of the average surface temperature during the wake-to-envelope transition than the one-step mechanism. The four-step mechanism has earlier instant of the wake-to-envelope transition than the one-step mechanism at low ambient temperature (e.g., 1200 K), but this difference between the two mechanisms diminishes when the ambient temperature is increased. The four-step mechanism has smaller mass burning rate for a wake flame (before the wake-to-envelope transition for the cases with an initial wake flame) but greater mass burning rate for an envelope flame (the case with an initial envelope flame, and after the wake-to-envelope transition for the cases with an initial wake flame) than the one-step mechanism. So, the overall mass burning rates for the two mechanisms might be close for the cases with an initial wake flame. The two mechanisms have small differences in the critical initial Damkohler number, although the critical initial Damkohler number for the four-step mechanism is always slightly smaller than that for the one-step mechanism.

For both envelope flame and wake flame, a region of positive peak values exists for the reaction rates for all the four steps; however, a region of negative peak values also exists only for the water-gas-shift step and the H-atom-recombination step, because there are negative components in their rates which are comparable to the positive components and have peak values in a region different from that for the positive components.

Lower ambient temperature yields later wake-to-envelope transition and smaller mass burning rate, due to the smaller Da_0 which favors a wake flame and also the slower heating of the droplet. Higher ambient pressure has greater overall mass burning rate

because of greater gas density and thus greater concentrations of reactants for a major part of the lifetime. However, higher ambient pressure with greater boiling point has smaller molar fraction of fuel vapor near the droplet surface in the early period with low surface temperature, which is the factor that tends to postpone the wake-to-envelope transition and decrease the mass burning rate in the early period, while the factor of greater gas density does otherwise. Greater ambient mass fraction of oxygen yields faster oxidation kinetics and greater Damkohler number. As the ambient mass fraction of oxygen increases, the instant of wake-to-envelope transition advances for an initial wake flame, and finally the initial flame becomes an envelope flame when the ambient mass fraction of oxygen exceeds some critical value. For an initial wake flame, the mass burning rate increases rapidly as the ambient mass fraction of oxygen increases. When the initial flame becomes an envelope flame, the mass burning rate still increases modestly with the increasing ambient mass fraction of oxygen.

As the critical initial Damkohler number varies with the ambient conditions, a correlation is developed for the critical initial Damkohler number in terms of the ambient temperature, ambient pressure, and ambient mass fraction of oxygen. A modified initial Damkohler number is defined based on the correlation so that it has a critical value independent on the ambient conditions.

Some important effects for convective fuel droplet burning have been examined in the literature, such as droplet internal circulation, variable properties, surface tension, and transient droplet heating. Compared with these effects, the effect of the chemistry model is smaller but still non-negligible. As the increase in the computational time is not demanding, the use of the four-step chemistry is more desirable than the one-step mechanism for a better approximation of the burning droplet behaviors.

References

- [1] S. Prakash, W.A. Sirignano, *Int. J. Heat Mass Transfer* 21 (1978) 885–895.
- [2] S. Prakash, W.A. Sirignano, *Int. J. Heat Mass Transfer* 23 (1980) 253–268.
- [3] A.Y. Tong, W.A. Sirignano, *Symp. (Int.) Combust.* 19 (1982) 1007–1020.
- [4] R.H. Rangel, A.C. Fernandez-Pello, *Combust. Sci. Technol.* 42 (1984) 47–65.
- [5] C.H. Chiang, M.S. Raju, W.A. Sirignano, *Int. J. Heat Mass Transfer* 35 (1992) 1307–1324.
- [6] Y. Aouina, U. Maas, *Combust. Sci. Technol.* 173 (2001) 1–23.
- [7] H.A. Dwyer, I. Aharon, B.D. Shaw, H. Niazmand, in: *Twenty-Sixth Symposium (International) on Combustion*, 1996, pp. 1613–1619.
- [8] H.A. Dwyer, B.D. Shaw, H. Niazmand, in: *Twenty-Seventh Symposium (International) on Combustion*, 1998, pp. 1951–1957.
- [9] V. Raghavan, V. Babu, T. Sundararajan, R. Natarajan, *Int. J. Heat Mass Transfer* 48 (2005) 5354–5370.
- [10] G. Wu, W.A. Sirignano, *Combust. Flame* 157 (2010) 970–981.
- [11] D.N. Pope, G. Gogos, *Combust. Flame* 142 (2005) 89–106.
- [12] D.N. Pope, D. Howard, K. Lu, G. Gogos, *AIAA J. Thermophys. Heat Transfer* 19 (2005) 273–281.
- [13] W.A. Sirignano, *Fluid Dynamics and Transport of Droplets and Sprays*, second ed., Cambridge University Press, 2010.
- [14] H.K. Chelliah, F.A. Williams, *Combust. Flame* 80 (1990) 17–48.
- [15] K. Seshadri, N. Peters, *Combust. Flame* 81 (1990) 96–118.
- [16] N. Peters, in: M.D. Smooke (Ed.), *Reduced Kinetic Mechanisms and Asymptotic Approximations for Methane–Air Flames*, Springer, 1991, pp. 48–67.
- [17] J.M. Card, *Combust. Flame* 93 (1993) 375–390.
- [18] E. Gutheil, *Combust. Flame* 93 (1993) 239–254.
- [19] A. Cuoci, M. Mehl, G. Buzzi-Ferraris, T. Faravelli, D. Manca, E. Ranzi, *Combust. Flame* 143 (2005) 211–226.
- [20] A. Neophytou, E. Mastorakos, R.S. Cant, *Proceedings of the Combustion Institute*, doi:10.1016/j.proci.2010.06.022.
- [21] J. Warnatz, in: W.C. Gardiner Jr. (Ed.), *Combustion Chemistry*, Springer-Verlag, 1984, pp. 197–360.
- [22] C.K. Westbrook, F.L. Dryer, *Prog. Energy Combust. Sci.* 10 (1984) 1–57.
- [23] C.L. Yaws, *Chemical Properties Handbook*, McGraw Hill, 1999.
- [24] S. Bretznajder, *Prediction of Transport and Other Physical Properties of Fluids*, Pergamon Press, 1971.
- [25] R.C. Reid, J.M. Prausnitz, T.K. Sherwood, *The Properties of Gases and Liquids*, third ed., McGraw-Hill, 1977.
- [26] G. Wu and W.A. Sirignano, *Proceedings of the Combustion Institute*, doi:10.1016/j.proci.2010.05.012.